Effects of Strain Path Changes on the Formability of Sheet Metals

JOSEPH V. LAUKONIS AND AMIT K. GHOSH

The effects of a change in strain path on the deformation characteristics of aluminum-killed steel and 2036-T4 aluminum sheets have been studied. These sheets were prestrained various amounts in balanced biaxial tension and the resulting uniaxial properties and forming limits for other loading paths were determined. In comparison to uniaxial prestrain the steel was found to suffer a more rapid loss in uniform strain upon the strain path change from biaxial to uniaxial. In contrast, the uniform strain in aluminum does not drop as rapidly after the same change. In keeping with this behavior, the forming limit diagram of steel is found to decrease with prestrain at a much faster rate than that of aluminum. Such effects can be explained in terms of the transition flow behavior of the metals occurring upon the path change. Thus, the path change produces strain softening and premature failure in steel, while causing additional strain hardening and consequent flow stabilization in aluminum.

FORMING limit diagrams (FLD),[1,2] which define maximum allowable strain levels during sheet metal forming, have found increased usage in sheet stamping analysis. These diagrams show the magnitude of major strain before the onset of a localized neck as a function of minor strain in the sheet surface (Fig. 1). Usually, strain paths during one step forming operations are nearly proportional, *i.e.* they maintain a nearly constant ratio of major to minor strain as indicated in Fig. 1. Laboratory punch stretching tests also produce such nearly linear strain paths,[3] and consequently laboratory FLDs match the practical ones quite well.

In practice, the stamping of sheet metal components often involves multiple operations. Such operations may vary from a draw-type (extension-contraction) to a stretch-type (extension-extension) deformation in the sheet plane. During stamping, certain material locations in a part may experience a change from one type of deformation to the other. In a single operation such changes are generally gradual; however, in a multiple operation abrupt changes can take place.

There is evidence in the literature[4,5] that changes in the mode of deformation can alter the formability of sheet steel. Biaxial prestraining has been found to reduce the uniaxial ductility of low carbon steel when compared with its ductility in continuous uniaxial tensile deformation.[4] It was shown that such effects might arise from increased hardening under biaxial tension, resulting in a premature loss of stability when the deformation mode is changed from biaxial to uniaxial tension. The forming limit diagrams presented by Kobayashi, Ishigaki and Abe[5] provide further support to this effect. In addition, they show that prior straining along a uniaxial tensile path enhances the subsequent biaxial ductility as measured from forming limit diagrams.

These effects appear to be important in sheet metal forming practice, particularly in the design of dies intended for multiple-stage stamping. Unfortunately, the foregoing references do not provide sufficient characterization of the useful formability parameters. The present study was undertaken, in part, to meet this goal, as well as to investigate possible differences in behavior between materials belonging to different crystallographic classes. Such a possibility was prompted by the earlier observation of increased strain hardening under biaxial tension (in comparison to the uniaxial case) occurring in ferrous materials, and a reverse behavior for nonferrous materials.[4]

Thus, the choice of a low carbon steel as a test material was natural. Aluminum was selected as a representative of the nonferrous group. The alloy chosen (commercial designation 2036-T4) possesses

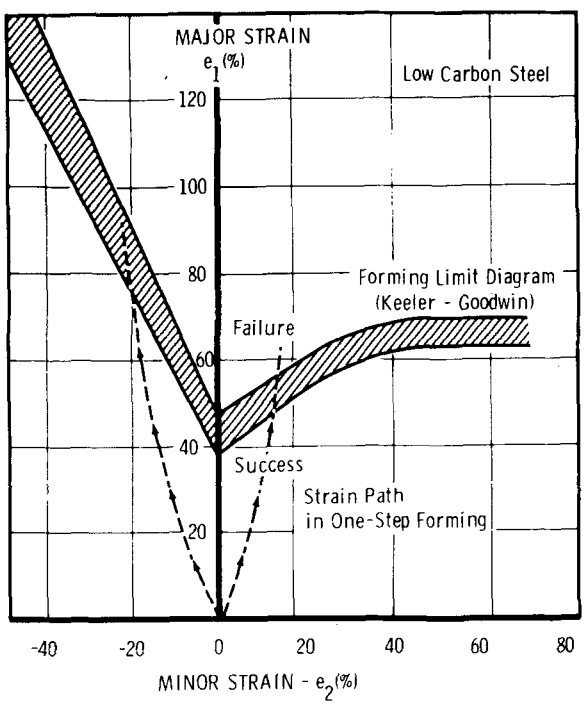

Fig. 1—Forming limit diagram and strain paths for one-step forming.

JOSEPH V. LAUKONIS is Senior Research Physicist, Physics Department, General Motors Research Laboratories, Warren, MI 48090, and AMIT K. GHOSH, formerly with General Motors Research Laboratories, is now a member of Technical Staff, Rockwell International Science Center, Thousand Oaks, CA 91360.

Manuscript submitted February 2, 1978.

ISSN 0360-2133/78/1211-1849$00.75/0
© 1978 AMERICAN SOCIETY FOR METALS AND THE METALLURGICAL SOCIETY OF AIME

Table I. Composition of Aluminum–Killed Steel

Pct C	0.047
Pct S	0.023
Pct P	0.002
Pct Mn	0.27
Pct Si	0.011
Pct Al	0.037
Pct N	59 ppm
Pct Fe	Balance

Table II. Composition of 2036-T4 Aluminum

Pct Cu	2.63
Pct Mn	0.27
Pct Mg	0.28
Pct Fe	0.22
Pct Si	0.33
Pct Al	Balance

a flow stress and strain hardening characteristics similar to those of low carbon steels. In contrast to steel which has a positive value of strain-rate hardening index, the rate sensitivity index of this aluminum is slightly negative. In addition, as shown by Hecker,[3] its FLD level is about half that of steel. Finally, its plastic anisotropy parameter, r, is less than unity while that of steel is greater.

EXPERIMENTAL

Material

The materials used in this study are: 1) a cold-rolled and annealed, aluminum-killed (A-K) steel sheet, 0.89 mm thick and 2) a precipitation hardenable aluminum–2.6 pct copper alloy (2036-T4), 0.97 mm thick sheet in a solution treated and naturally aged condition. The chemical composition of the A-K steel is given in Table I while that of the 2036-T4 aluminum is given in Table II.

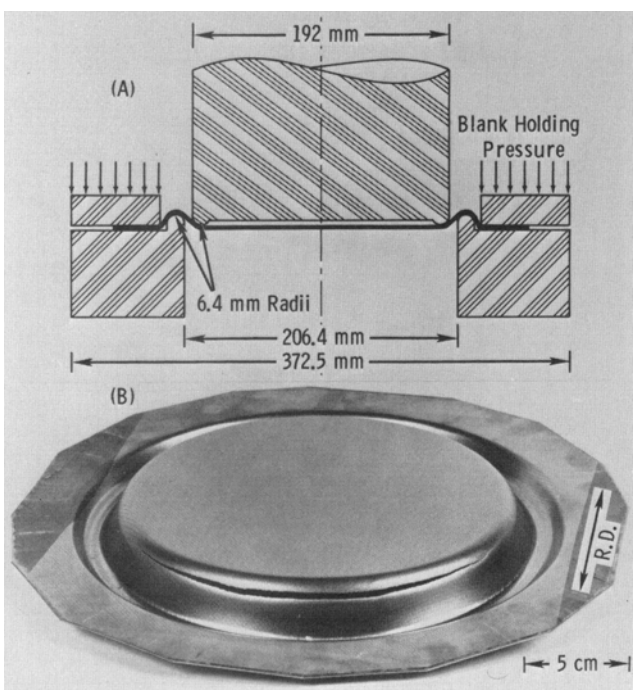

Fig. 2—Details of the prestraining operation: (*a*) Diagram of punch and die set, (*b*) a prestrained blank.

The Prestraining Operation

The test materials were biaxially prestrained on a 445 kN (50 tonne) hydraulic press using a punch and die set of circular symmetry. The metal blank for prestraining was a 305 mm diam, roughly circular disc photoprinted with a 1.92 mm diam circle grid pattern. A schematic diagram of the punch and die set with the metal blank in position is shown in Fig. 2(*a*). The blank was firmly clamped with a holding force of about 25 tonnes over a 6.4 mm radii drawbead and was stretched, generally to failure, over the end of a 192 mm diam right-circular cylindrical punch at a punch displacement rate of approximately 10 mm/min (also the rate for subsequent uniaxial tests).

A typical prestrained blank is shown in Fig. 2(*b*). The useful part of the blank is the central circular portion about 180 mm in diam showing balanced biaxial deformation. The magnitude of prestrain was determined from the photogrid along both the rolling and transverse directions. Use of different lubricants and variations in the corner radius of the punch with appropriate inserts produced the different amounts of prestrain listed in Table III. Sets of prestrained blanks were thus prepared for subsequent tensile and formability studies.

Tensile Tests

Standard E-8 (ASTM) specimens with a gage length of 50.8 mm and a width of 12.7 mm were cut at 0, 45, and 90 deg to the sheet rolling direction for the as-received steel and aluminum and for each of their prestrained states. These were subsequently tested on an Instron machine at a crosshead speed of 10 mm/min (strain rate $\sim 3 \times 10^{-3}$ s^{-1}) using a 50.8 mm gage length LVDT extensometer, and a continuous load-elongation record was maintained during the test. The load-elongation plots were used to determine true stress (σ) as a function of true strain (ϵ). The strain hardening exponent, n, and strength coefficient, K, that fit the empirical hardening law $\sigma = K\epsilon^n$, were determined from log σ *vs* log ϵ plots.

Tensile specimens photogridded prior to testing were used in the measurement of plastic anisotropy.

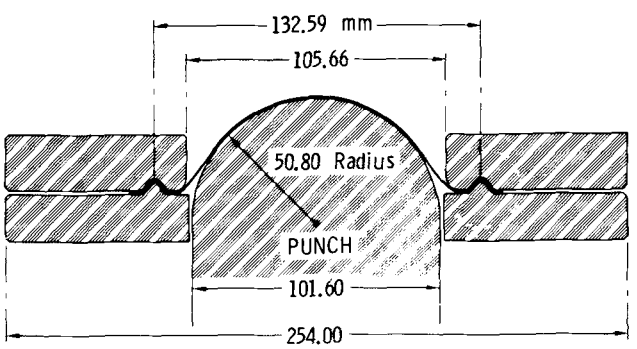

Fig. 3—The punch test apparatus.

Table III. Balanced Biaxial Prestrains

Material	Designation	Effective Prestrains†
A-K Steel	A*	0.070
	B	0.081
	C	0.094
	D	0.107
	E*	0.152
	F*	0.271
2036-T4 Aluminum	A	0.019
	B*	0.037
	C	0.046
	D*	0.062
	E*	0.101
	F	0.108
	G	0.119
	H	0.129
	I	0.145
	J*	0.197
	K	0.227
	L	0.244
	M	0.253
	N	0.266

*Forming limit diagrams were constructed for these states only. For the remaining states a limited number of samples were prestrained for additional data on the biaxial flow curve and r-value measurements.

†Corrected for Anisotropy using the formula:

$$\epsilon_e = 2\sqrt{(2 + r/1.5(1 + r))}\ \epsilon_1$$ where ϵ_e = effective prestrain, and ϵ_1 = unidirectional prestrain.

The plastic anisotropy parameter, r, defined by $r = |\epsilon_w|/(\epsilon_l - |\epsilon_w|)$, where ϵ_w = true width strain and ϵ_l = true longitudinal strain, was calculated from measurements of longitudinal and width strains from these grids. Such measurements were confined to areas of uniform deformation.*

*In prestrained specimens showing small amounts of uniform strain, measurements were made from areas with slight nonuniformity in strain, yet close enough to the free surface of the specimens to ensure a uniaxial stress-state.

The tensile properties of the as-received A-K steel and 2036-T4 aluminum are reported in Table IV while average tensile properties of their prestrained states are given in Tables V and VI respectively.

Formability Tests

Forming limit diagrams (FLD) for the as-received and prestrained materials were determined according to a procedure reported by Hecker.[3] The procedure consists of clamping rectangular sheet blanks of various widths (each 152 mm long) over a lockbead and stretching to failure over a 101.6 mm diam hemispherical punch (Fig. 3). Blank widths were 51, 76, 89, 102, 114, 127, and 152 mm. Three additional square blanks (152 × 152 mm) were stretched with three different lubricants to generate more positive minor strains at failure.

The FLDs were constructed by 1) measuring both major and minor strains from regions just outside visible necks or fractures, 2) plotting these strain combinations on a plot of major strain *vs* minor strain, and 3) drawing a limiting curve to separate the acceptable from the visually unacceptable strain combinations. Gridded tensile specimens provided additional data points for the FLDs. The FLDs for the as-received steel and the various prestrain states are shown in Fig. 4 while the corresponding plots for the aluminum are shown in Fig. 5.

RESULTS AND DISCUSSION

The Effects of Prestrain on FLDs

It should be noted that Figs. 4 and 5 represent accumulated strains from two deformation steps, *i.e.* prestraining and subsequent straining. These plots readily show if a certain combination of major and minor strains is achievable by either a single or a double strain path. For example, as futher illustrated in Fig. 6 for 2036-T4 aluminum, strain combinations within Region 'B' were not attainable in a single-step operation but are attainable after a biaxial prestrain $\overline{OP}$. Conversely, strain combinations within region 'C' which were attainable in a single-step operation

Table IV. Tensile Properties of the As-Received Materials

(*a*) A-K Steel

Direction*, deg	Yield Strength†, MPa	Uniform Strain, Pct	Total Strain-Pct Over 50.8 mm	n	K, MPa	r	Δr‡
0	154	27.6	40.8	0.242	501	1.74	
45	165	25.7	38.9	0.229	522	1.79	0.23
90	156	26.5	42.4	0.234	488	2.29	
Average¶	160	26.4	40.3	0.234	508	1.90	

(*b*) 2036-T4 Aluminum

Direction*, deg	Yield Strength†, MPa	Uniform Strain, Pct	Total Strain-Pct Over 50.8 mm	n_1§	K_1§	n_2#	K_2#	r	Δr‡
0	175	17.9	21.0	0.296	689	0.224	591	0.62	
45	182	18.5	22.2	0.277	620	0.225	576	0.61	−0.03
90	180	17.8	21.0	0.285	621	0.236	584	0.54	
Average	180	18.1	21.6	0.284	638	0.228	582	0.59	

*Directions are measured relative to the rolling direction of the as-received sheet.

†Yield strength at 0.2 pct plastic strain.

‡$\Delta r = r_0 + r_{90} - 2r_{45}/2$.

¶ All properties are averaged according to $X_{avg} = x_0 + 2x_{45} + x_{90}/4$.

§ Applicable to the strain range from 0.06 to 0.15.

#Applicable to the strain range from 0.15 to 0.20.

Table V. Average Values¶ of Tensile Properties of Prestrained A-K Steel

Prestrain State*, Effective Strain	Yield Strength†, MPa	Uniform Strain, Pct	Total Strain§, Pct	n	MPa	r	Δr‡
A(0.070)	300	13.9	32.5	0.101	431	1.71	0.67
C(0.094)	356	0.5	15.9	–	–	1.12	0.06
D(0.107)	350	0.3	17.8	–	–	1.34	0.02
E(0.152)	392	0.4	10.2	–	–	–	–
F(0.271)	439	0.4	4.9	–	–	–	–

¶, †, and ‡See Table IV.

*A limited number of samples were prestrained to state *B*(0.081) for additional data on biaxial hardening and plastic anisotropy.

§ Over 50.8 mm gage length.

are no longer attainable after the same prestrain. Figures 4 and 5 thus indicate that while aluminum exhibits a beneficial influence of prestrain on the overall FLD for $e_2 \geq 0$, no such effect is exhibited by steel. In fact, large biaxial prestrain appears to be detrimental to steel's formability for all strain states.

An additional feature of plotting accumulated strains (Figs. 4 and 5) is that, the FLD minima shift in the minor strain direction by an amount equal to the minor strain component (e_2) of the prestrain. This is because the origin for the subsequent strain is now fixed at the strain coordinates of the prestrained state. A more important observation is however, that the level of FLD minima for aluminum is nearly unchanged while that for steel decreases with increasing prestrain. This supports the observation that biaxial prestrain is detrimental to the formability of steel.

Table VI. Average Values¶ of Tensile Properties of Prestrained 2036-T4 Aluminum

Prestrain State*, Effective Strain	Yield Strength†, MPa	Uniform Strain, Pct	Total Strain§, Pct	n#	K#, MPa	r	Δr‡
A(0.019)	223	17.4	18.8	$n_1 = 0.212$ $n_2 = 0.165$	$K_1 = 594$ $K_2 = 533$	0.61	0
B(0.037)	231	15.2	17.0	0.179	524	0.58	0.14
C(0.046)	258	13.9	15.0	0.156	539	0.60	0.04
D(0.062)	284	10.8	12.2	0.129	540	0.55	-0.13
E(0.101)	302	8.5	9.8	0.112	535	0.57	-0.02
J(0.197)	348	5.5	6.1	0.072	512	0.60	-0.01
L(0.244)	357	4.3	5.0	0.069	514	0.67	-0.15

¶ and ‡See Table IV.

*A limited number of samples were prestrained to states F(0.108), G(0.119), H(0.129), I(0.145), K(0.227), M(0.253), and N(0.266) for additional data on biaxial hardening and plastic anisotropy.

†Yield strength as per special construction (Fig. 9).

§ Over 50.8 mm gage length.

#n_1 and K_1 are applicable for true strains from 0.025 to 0.10 while n_2 and K_2 are for strains from 0.1 to 0.16.

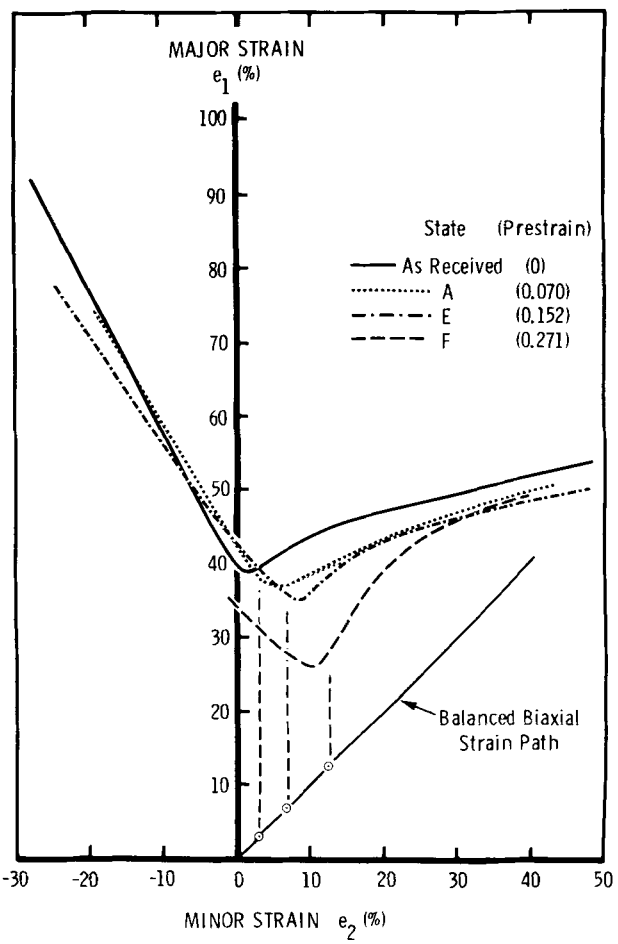

Fig. 4—Forming limit diagrams for aluminum-killed steel as a function of balanced biaxial prestrain.

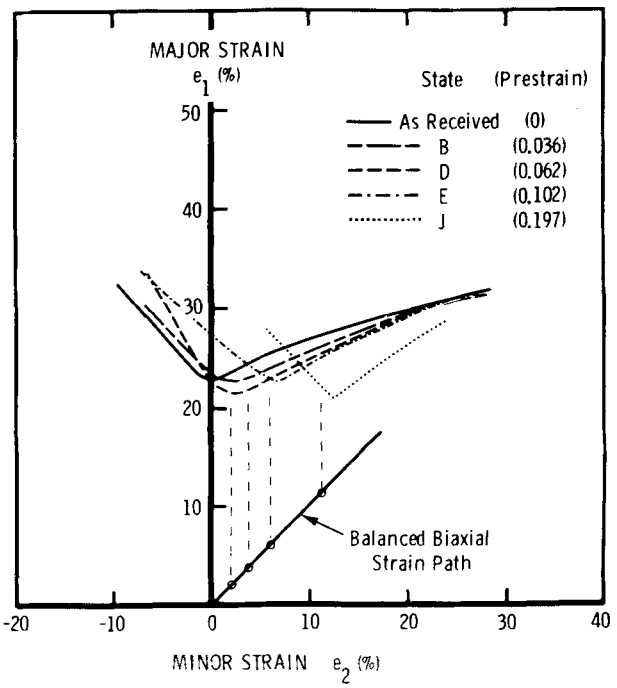

Fig. 5—Forming limit diagrams for 2036-T4 aluminum as a function of balanced biaxial prestrain.

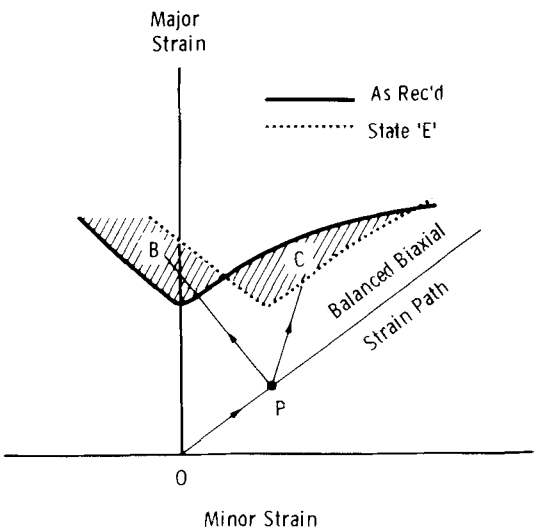

Fig. 6—2036-T4 aluminum, schematic forming limit representation of i) strain states (Field B) attainable after balanced biaxial prestrain (OP) which were not attainable in a single-step operation, and ii) strain states (Field C) not attainable after the biaxial prestrain, which were previously attainable.

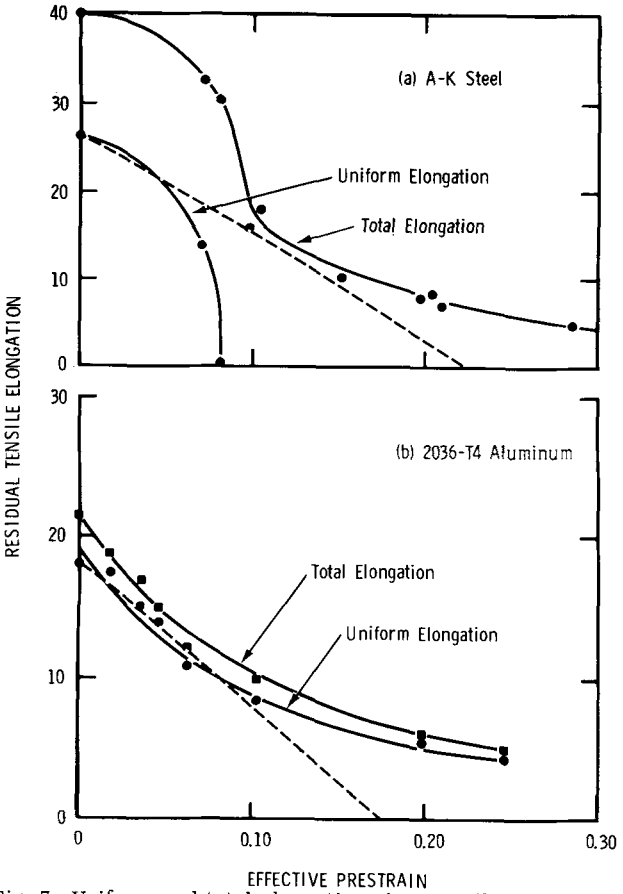

Fig. 7—Uniform and total elongations in a tensile test (over a 50.8 mm gage length) after biaxial prestraining, plotted as a function of effective prestrain. (*a*) A-K steel, (*b*) 2036-T4 aluminum. (The dashed curves represent the expected behavior of uniform strain if prestrain was uniaxial.)

Residual formability, *i.e.* the strain difference between the prestrain state and the appropriate FLD, of both steel and aluminum is always reduced by prestrain. The reduction is more rapid for the steel than for the aluminum. Thus, while the as-received steel starts out being about twice as formable as the as-received aluminum, the difference becomes progressively smaller with increased balanced biaxial prestrain.

Changes in Tensile Elongations Caused by Prestraining

In Fig. 7(*a*) and (*b*) tensile elongations for respectively, A-K steel and 2036-T4 aluminum are plotted as a function of balanced biaxial prestraining. Substantial differences exist in the response of the two materials, especially with regard to uniform elongation. For steel, biaxial prestraining causes the uniform elongation to drop to nearly zero at an effective prestrain of about 0.08. Had the prestrain been uniaxial, residual uniform elongation would decrease along the dashed curve in the figure and would not become zero until prestrain was 0.223. Thus, the loss in (subsequent) uniaxial flow stability due to biaxial prestrain is significant. The total elongation does not drop as rapidly because elongation beyond maximum load is controlled to a large extent by strain rate sensitivity,* which is relatively unaffected by prestrain.[7]

*A positive strain-rate sensitivity is largely responsible for the substantial post-uniform elongation of A-K steel.[6]

In contrast to the steel behavior, the residual uniform flow capability of 2036-T4 aluminum is greater when the prestrain is biaxial (Fig. 7(*b*)), *i.e.*, more uniform elongation can now be obtained in comparison to the case of uniaxial prestrain. The postuniform elongation is very small for this alloy because it has a negative strain-rate sensitivity[6] which again is relatively unaffected by prestrain.

The changes in uniform elongation just discussed are further supported by a precipitous drop (after a strain of 0.07) in n for prestrained steel and a much slower drop for prestrained aluminum (see Tables V and VI). Note that the parabolic hardening law does not describe the behavior of aluminum very well; double-n hardening behavior is exhibited by aluminum in both as-received and prestrained conditions. Larger prestrains apparently take the material beyond the first stage of hardening, which is therefore absent from their stress-strain curves.

Reconstructing Biaxial Flow Curves from Tensile Tests of Prestrained Materials

The nature of the effect of a strain path change is best understood by examining tensile stress-strain data in some detail. This will be done in discussing Fig. 8(*a*) and (*b*) which respectively show both uniaxial and biaxial hardening curves for A-K steel and

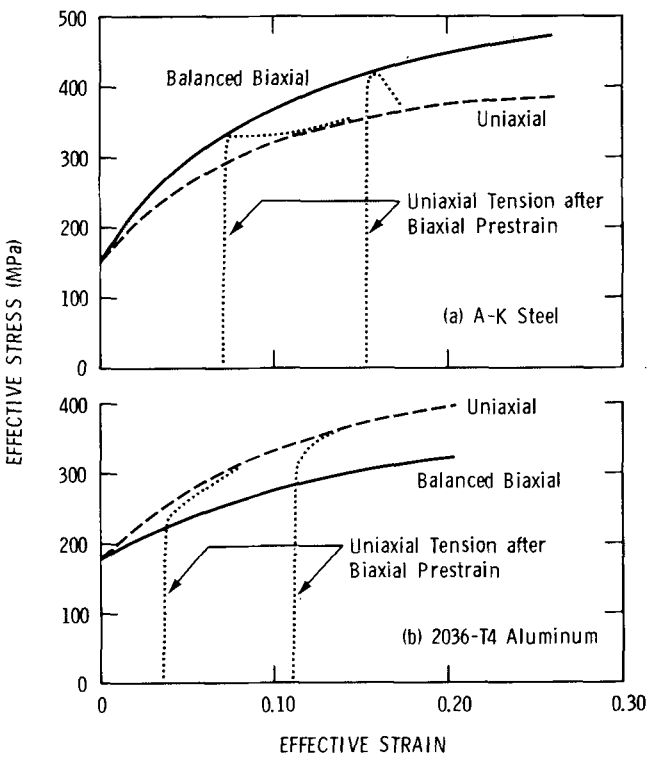

Fig. 8—The uniaxial and biaxial flow curves of: (*a*) A-K steel, and (*b*) 2036-T4 aluminum, along with several strain path change stress-strain curves for each material (shown as dotted lines).

2036-T4 aluminum along with two complete tensile curves of biaxially prestrained states.

The uniaxial curves in Fig. 8 are obtained directly from tensile test data of the respective materials in their as-received state. The biaxial curves represent the loci of tensile yield points of biaxially prestrained materials. This method of indirect reconstruction has been used to determine "extended stress-strain curves" in metal forming processes where flow stress measurement is extremely complicated, such as in wire drawing, rolling, extrusion, and so forth.[8] The implicit assumption of this method is that the flow stress before unloading (here, from the biaxially prestrained state) would have to be reached first in order to resume plastic flow. On this basis, the yield point (0.2 pct offset plastic strain) of biaxially prestrained A-K steel was selected as the flow stress on the biaxial stress-strain curve, and the locus of such points gave the biaxial stress-strain curve in Fig. 8(*a*).

The use of this method to the tensile results of 2036-T4 aluminum is complicated by the presence of the Bauschinger effect; *i.e.* a drop in the initial yield stress upon change of stress state. While this effect is known to be largest for a complete stress reversal,[9] it is substantial even when the stress state is changed from biaxial to uniaxial. Thus, the above method to reconstruct the biaxial flow curve of 2036-T4 aluminum would be unreasonable.

An indirect construction shown in Fig. 9, is used in this case to obtain the yield points of prestrained states. The first attainment of parabolic hardening in the tensile test of the prestrained state was assumed to represent the characteristic of gross plastic flow. Thus, a back extrapolation of the initial linear slope in the log σ *vs* log ϵ plot in Fig. 9 may be regarded as the stress-strain curve that would have been obtained if the Bauschinger effect was absent. The intersection of this line with the $\epsilon_p = 0.002$ line thus gives the desired biaxial flow stress (yield stress) as shown on Fig. 9. The yield stresses so obtained are subsequently used to construct the biaxial flow curve shown in Fig. 8(*b*).

Biaxial-n and K values (for $\sigma_e = K\epsilon_e{}^n$) for the two materials are obtained from logarithmic plots of the biaxial flow curves in Fig. 8. Such plots are shown in Fig. 10 (along with their uniaxial counterparts) and the n and K values obtained therefrom are tabulated in Table VII. From these it can be seen that not only biaxial strength, but also biaxial n for steel is

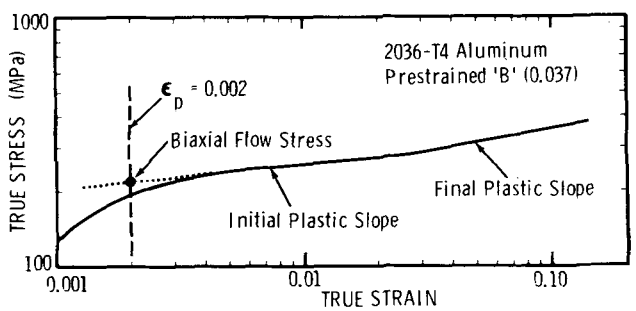

Fig. 9—Logarithmic plot of true stress *vs* true strain from a tensile test of biaxially prestrained 2036-T4 aluminum (state 'B' (0.037), sample cut along rolling direction), illustrating the construction used to obtain biaxial flow stresses.

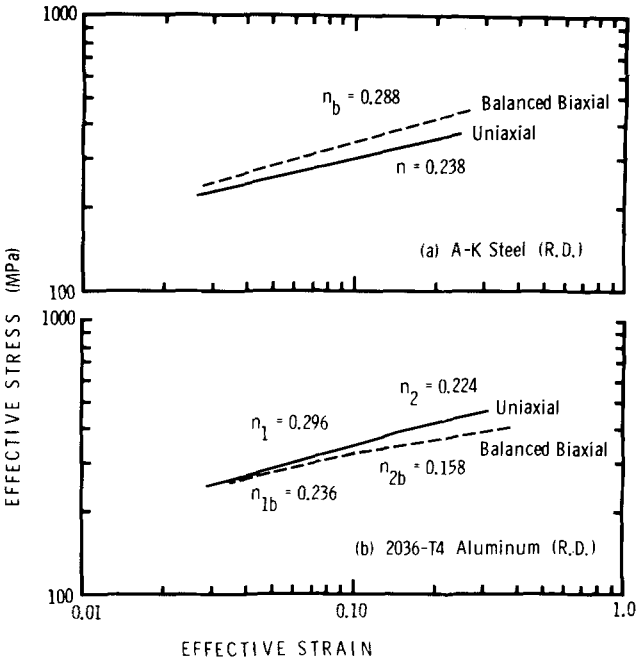

Fig. 10—Logarithmic plots of effective stress *vs* effective strain under uniaxial and balanced biaxial tension for: (*a*) A-K steel, (*b*) 2036-T4 aluminum.

greater than its uniaxial values. Conversely, biaxial strength and n for aluminum are less than its uniaxial values, respectively. Furthermore, steel continues to exhibit a single n behavior while aluminum shows a double n behavior under biaxial tension.

The Stability of Transition Flow for a Change of Strain Path

Probable change of strain path effects follow from the relative positions of the uniaxial and biaxial flow curves in Fig. 8. The important difference to be noted is that biaxial prestraining renders the steel considerably stronger than expected on the basis of the uniaxial hardening curve, while the same prestraining makes the aluminum weaker. It can be noted that stresses and strains are expressed in terms of their effective values using Hills' anisotropy-corrected formulation.[10] However, it should be observed that the results are not significantly altered without this correction.

Biaxially prestrained steel, which exhibits additional hardening on yielding (Fig. 8(*a*)), undergoes strain softening during subsequent tensile deformation. This

Table VII. Strain Hardening Exponents (n_b) and Strength Coefficients (K_b) for A-K Steel and 2036-T4 Aluminum Under Biaxial Tension

Material	Direction, deg	n_b	K_b, MPa
A-K Steel	0	0.288	688
	45	0.302	738
	90	0.241	646
2036-T4 Aluminum	0	0.236/0.158*	558/464*
	45	0.208/0.168	505/458
	90	0.218/0.182	522/481

*The larger n and K values are valid for $0.02 \leq \epsilon_e \leq 0.10$. The smaller values apply for $0.10 \leq \epsilon_e \leq 0.20$.

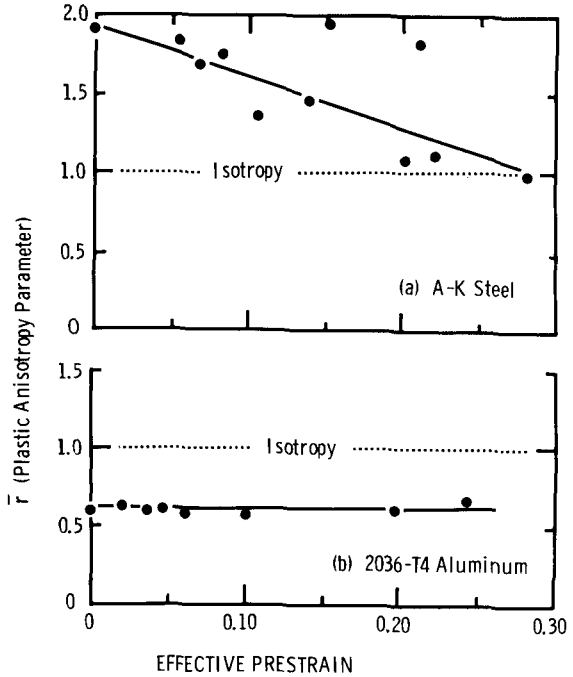

Fig. 11—Average values of the plastic anisotropy parameter as a function of effective prestrain: (*a*) A-K steel, (*b*) 2036-T4 aluminum.

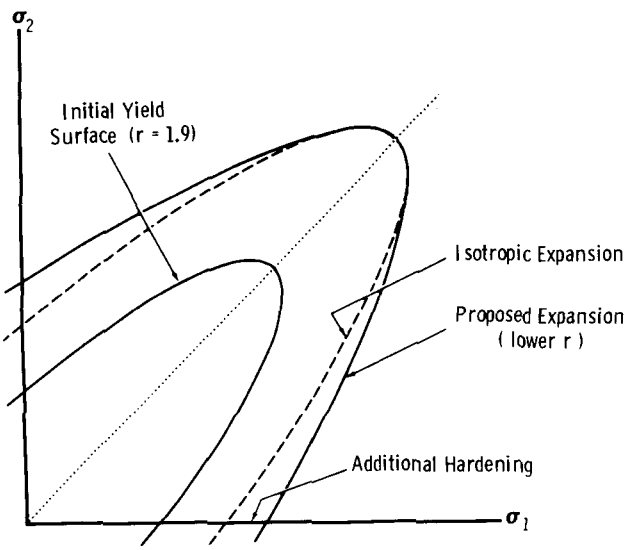

Fig. 12—Schematic change in yield surface afer balanced biaxial prestraining of A-K steel.

results from an approach toward the uniaxial curve which represents the equilibrium state during the second deformation. Consequently, for all but the lowest prestrain states, the instability condition, $d\sigma/d\epsilon = \sigma$, is satisfied and premature necking occurs. It is this strain softening during the transition flow that produces the precipitous drop in uniform strain that has been previously noted.

In the case of the aluminum alloy, yielding occurs at a lower stress and therefore subsequent deformation is marked by a rise in the strain hardening rate. Clearly such a change gives rise to additional flow stability which in turn gives rise to the previously noted larger uniform strain. This type of behavior has been previously observed in 70:30 brass.[4] For commercial purity aluminum, however, only a small dependence of strain hardening on the imposed stress-state was found,[4] in contrast to the present results on 2036-T4. While present plasticity theories do not take such behavior into account, there is additional evidence in the literature for its support, *viz*, Yoshida *et al*,[11] Davis,[12] and Woodthorpe and Pearce.[13]

Changes in Anisotropy with Prestrain

The increased hardening in biaxial tension for steel is simultaneously associated with a drop in plastic anisotropy parameter, r, as shown in Fig. 11(*a*). In spite of the large scatter in the data, it appears that biaxial prestrain renders steel more isotropic. From a microstructural point of view, the "wavy glide" nature of slip in steel is known to produce a dense dislocation cell structure. Additionally, certain latent slip systems are believed to become activated under biaxial loading.[11,14] This may explain observed increased hardening under biaxial stretching. It is also possible that a more equiaxed dislocation cell structure develops under biaxial stresses,[15] and partially annihilates the plastic anisotropy causing r to drop from near 2.0 toward unity with prestrain. Schematic expansion and distortion of the yield surface as shown in Fig. 12 illustrate this anisotropy change with increased hardening in the subsequent uniaxial tensile yield (for small offset). While this increased hardening does not persist up to larger strains, it certainly acts in addition to isotropic hardening.

Anisotropy change, if any, in the case of the aluminum is not readily detectable (Fig. 11(*b*)).

CONCLUSIONS

1) The residual formability of both A-K steel and 2036-T4 aluminum is reduced in proportion to the magnitude of balanced biaxial prestrain.

2) For 2036-T4 aluminum the plane strain level of the forming limit diagram remains unchanged by balanced biaxial prestrain. The result of this behavior is to make some draw-type strain combinations which were not attainable in a one step deformation process, become available in a two-step process. Conversely, some stretch-type combinations which were available to the as-received material become unattainable for a two step process.

3) For A-K steel, the biaxial hardening curve obtained by joining the tensile yield points of prestrained states, shows increased hardening under biaxial loading in comparison to uniaxial deformation. It also appears that biaxial n for steel is greater than its uniaxial value. Therefore, the strain softening which occurs upon a strain path change toward uniaxial produces a precipitous loss in ability for uniform deformation for the balanced biaxially prestrained steel.

4) For 2036-T4 aluminum, the biaxial hardening curve, also obtained by joining the tensile yield points of prestrained states, shows less hardening under biaxial loading than under uniaxial loading. Also biaxial n for aluminum appears to be lower than its uniaxial value. Therefore, the increased strain hardening which occurs upon a strain path change toward uniaxial produces an increased ability for subsequent uniform deformation of the prestrained aluminum.

5) For A-K steel, the magnitude of the plastic anisotropy parameter, r, drops with prestrain suggesting a partial annihilation of a preferred grain orientation by the strain path change. The same strain path change produced no measurable change in r for 2036-T4 aluminum.

REFERENCES

1. S. P. Keeler: Paper No. 680092, Presented at the SAE Congress, Detroit, January 1968.
2. G. M. Goodwin: Paper No. 680093, Presented at the SAE Congress, Detroit, January 1968.
3. S. S. Hecker: *Proc. 7th Biennial Congress of IDDRG*, p. 5.1, Amsterdam, October 1972.
4. A. K. Ghosh and W. A. Backofen: *Met. Trans.*, 1973, vol. 4, p. 113.
5. T. Kobayashi, H. Ishigaki, and T. Abe: *Proc. 7th Biennial Congress of IDDRG*, p. 8.1, Amsterdam, October 1972.
6. A. K. Ghosh: *J. Eng. Mater. Technol.*, 1977, vol. 99, p. 264.
7. A. Saxena and D. A. Chatfield: Paper No. 760209, Presented at the SAE Congress, Detroit, February 1976.
8. A. B. Watts and H. Ford: *Proc. Inst. Mech. Eng. (London)*, 1952-53, vol. 1B, p. 448.
9. E. Shiratori and K. Ikegami: *J. Mech. Phys. Solids*, 1968, vol. 16, p. 373.
10. R. Hill: *The Mathematical Theory of Plasticity*, p. 318, Oxford University Press, London, 1967.
11. K. Yoshida, K. Miyauchi, A. Tajikawa, T. Iwasaki, and S. Mizunuma: *Sci. Pap. Inst. Phys. Chem. Res.*, 1967, vol. 61, p. 119.
12. E. A. Davis: *J. Appl. Mech.*, 1943, vol. 10, p. A-187.
13. J. Woodthorpe and R. Pearce: *Int. J. Mech. Sci.*, 1970, vol. 12, p. 341.
14. U. F. Kocks: *Met. Trans.*, 1970, vol. 1, p. 1121.
15. S. R. Rouze: Unpublished research, General Motors Research Laboratories, 1974.